

Cyclic Oxidation Behavior of the Super Austenitic Stainless Steel 904L in Air at 500–650 °C

Manishkumar K. Singh¹ · Sharvan Kumar¹ · Om Prakash Sinha¹ · Vakil Singh¹ · Girija Shankar Mahobia¹

Received: 9 October 2019 / Accepted: 10 March 2020 / Published online: 27 March 2020
© The Indian Institute of Metals - IIM 2020

Abstract Cyclic oxidation behavior of the super austenitic stainless steel 904L was studied for 100 h over the intermediate temperature range from 500 to 650 °C in air. The oxidized surfaces and cross sections of the oxidized samples were examined by scanning electron microscope (SEM–EDS), X-ray diffractometer and electron probe micro analyzer. The weight gain was found to follow nearly parabolic rate law. At 500 and 550 °C, there was rapid weight gain up to the initial 5 h of exposure, whereas the rapid weight gain at 600 and 650 °C was up to 10 and 25 h of exposure, respectively. The weight gain was drastically reduced during the later stage of exposure. Since the formed scales were thin, strong peaks of austenite (γ)-matrix were observed in all the exposed samples. There was formation of thin layer of Cr_2O_3 on the specimens exposed at 500 and 550 °C. Also, there was heterogeneous formation of iron oxides in some regions. The exposure at higher temperatures of 600 and 650 °C led to the formation of different spinels of oxides such as FeCr_2O_4 , NiCr_2O_4 , FeNi_2O_4 and others, along with Cr_2O_3 and Fe_2O_3 oxides.

Keywords Super austenitic 904L · Oxidation kinetics · XRD · SEM–EDS · EPMA analysis

1 Introduction

Super austenitic stainless steels (SASS) possess outstanding oxidation and corrosion resistance over a wide range of temperature. These high-performance steels differ substantially from the conventional grades of stainless steel with respect of their high content of alloying elements Cr, Ni, Mo, Cu, Mn and a small amount of Si which enhances their strength as well as oxidation resistance at elevated temperatures [1]. These steels are known as Fe–Ni–Cr grade [2] and rely on the formation of a protective chromium-rich oxide scale with very low porosity, good adherence, high mechanical as well as thermodynamic stability and slow growth rate [3]. The most commonly used super austenitic stainless steels include 904L, 254 SMO, 654 SMO, AL-6XN, SANICRO-25 and 28, etc [4].

Earlier studies on majority of SASS have focused mainly on high-temperature deformation/precipitation behavior between 650 and 1000 °C [5]. The 904L steel is a SASS, designed for an intermediate level of oxidation and corrosion resistance up to 480 °C [6]. It contains a high level of Cr and Ni, in addition to Mo and Cu which provide corrosion resistance in certain media. The 904L steel is used widely in situations where corrosion resistance of the AISI 317L and 316L stainless steels is not up to the mark [7–9]. Some major uses of the SASS 904L include wiring in electrostatic precipitators, oil refinery components, gas scrubbing plants, seawater cooling devices, pulp, and paper processing industries, sulfuric, phosphoric and acetic acid processing plants owing to its good corrosion resistance, excellent stability, high strength, and weldability [4]. The standard heat treatment of the SASS 904L is solutionizing at 1050–1150 °C and water quenching.

Cao and Norell [10] compared oxidation behavior of the 304L and 904L stainless steels in humid air over the

✉ Manishkumar K. Singh
manishkumarsingh@gmail.com

¹ Department of Metallurgical Engineering, Indian Institute of Technology (Banaras Hindu University), Varanasi, India

temperature range of 450–600 °C and observed that oxidation resistance of the 904L was much higher than that of 304L. However, when the nitrogen content of the two steels was increased to a higher level of 10–20 at% through plasma nitriding, there was a reverse trend in oxidation resistance of the two steels. Oxidation resistance in humid air in the temperature range of 450–600 °C, under isothermal condition up to 168 h, was found to be lower for the 904L steel as compared with that of the 304L, due to short range ordering between chromium and nitrogen atoms and less availability of free chromium to form protective oxide of Cr₂O₃. This study was carried out to evaluate their applicability as automobile exhaust; however, for such applications it is more rational to evaluate oxidation resistance against cyclic oxidation rather than under isothermal condition.

As no report was available on cyclic oxidation behavior of the SASS 904L in air from 500 to 650 °C in open literature, the present investigation was undertaken to study oxidation kinetics of this steel under thermal cycling and characterize the morphology of the oxidized samples exposed for 100 h at four different temperatures of 500, 550, 600 and 650 °C in still air.

2 Experimental Procedures

2.1 Material

The SASS 904L was procured from M/s Bharat Aerospace Agency, Mumbai, as hot rolled rods of 16 mm diameter. Its chemical composition is presented in Table 1. Disk-shaped specimens of 14.5 mm diameter and 5 mm thickness were machined, polished, solution treated at 1100 °C for 1 h and quenched in water. The solution-treated samples were mechanically polished on emery papers and subsequently on velvet cloth using alumina powder and etched with aqua regia to reveal the microstructure. The hardness of the solution-treated sample was measured as 78 HRB. As most of the industrial components are fabricated by machining with surface roughness of about #600 grit, the disk-shaped samples for oxidation study were mechanically polished to comparable roughness, from practical point of view.

2.2 Oxidation Tests

Cyclic oxidation tests were performed in still air atmosphere at 500, 550, 600 and 650 °C up to 100 h in 15

cycles, in a muffle furnace. Each sample was kept in individual silica crucible and weighed before and after the cyclic oxidation test. The temperature of the furnace was controlled within ± 2 °C. The initial set of 5-cycles with 1 h soaking in each cycle at the test temperatures was followed by 4-cycles of 5 h soaking, 3-cycles of 10 h soaking and rest 3-cycles of 15 h soaking, and cooling to room temperature. The furnace was maintained at the temperature of exposure and the samples were directly loaded or taken out within a few seconds to ensure quick heating/cooling. The weight change was measured using an Axis electronic balance of 0.1 mg accuracy and after each set of cycles referred to above, till 100 h of exposure.

2.3 Characterization of Oxidized Surface

The oxidized/exposed samples were ultrasonically cleaned to remove any dirt/foreign particales from the surface as they charge during SEM examination and adversely affect the quality of the image. The surface morphology and compositional variation of the oxidized samples were examined by scanning electron microscopy (SEM, FE-SEM, Carl Zeiss, Sigma) and EDS (Oxford instruments-INCAx). The oxidation products were characterized by XRD (Rigaku MiniFlex-600) having a Cu-K α ($\lambda = 0.15406$ nm source) with scan rate of 10°/min. The cross sections of the oxidized samples were analyzed using Electron Probe Micro Analyzer (CAMECA SXFive) for elemental distribution across the oxidized scales and the base material.

3 Results

3.1 Microstructure Characterization

Optical micrograph of the solution-treated specimen of the SASS 904L is displayed in Fig. 1 showing single-phase microstructure with equiaxed grains of ≈ 40 μm mean intercept length and annealing twins in some grains.

3.2 Oxidation Kinetics

Oxidation kinetics of the SASS 904L is shown in Fig. 2 by plots of weight gain (ΔW) versus time of exposure (t) for 100 h at 500, 550, 600 and 650 °C in 15 cycles, in still air. After a rapid linear increase in ΔW in the beginning, a nearly parabolic behavior is observed, indicating good

Table 1 Chemical composition of the 904L steel (wt%)

C	Mn	Si	P	S	Ni	Cr	Cu	Mo	Fe	N
0.014	1.45	0.38	0.0024	0.02	24.1	19.95	1.59	4.02	Bal.	0.062

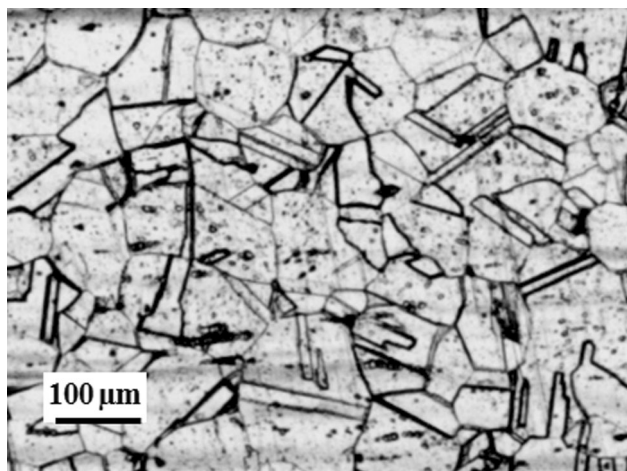


Fig. 1 Optical micrograph showing microstructure of the SASS 904L solution treated at 1100 °C for 1 h and water quenched

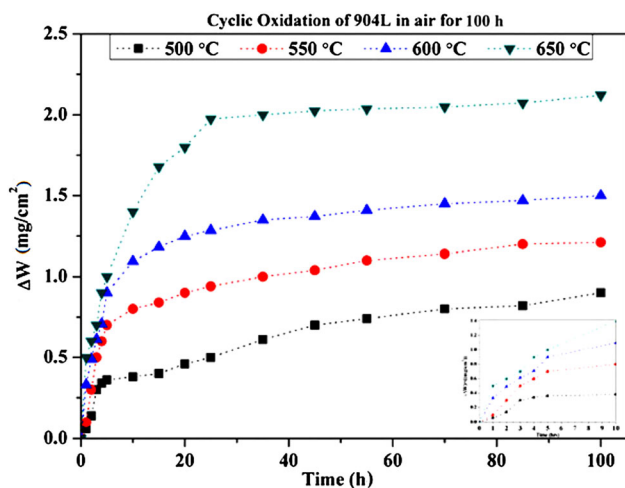


Fig. 2 Weight change (ΔW) per unit area during oxidation of the SASS 904L in air at 500, 550, 600 and 650 °C up to 100 h

oxidation resistance of this steel. The relationship between ΔW and t is shown in Eq. 1.

$$(\Delta W)^2 = k_p t + C \tag{1}$$

where ΔW is weight gain per unit area (mg/cm^2), k_p is parabolic rate constant in $\text{mg}^2 \text{cm}^{-4} \text{h}^{-1}$, t is oxidation time in h and C is a constant.

It is evident from Fig. 2 that there is highest weight gain in the sample exposed at 650 °C for 100 h. The values of k_p corresponding to different temperatures of exposure are presented in Table 2. ΔW progressively increases at an increasing rate, with rise in temperature of exposure from 500 to 650 °C. The data points of weight gain corresponding to different temperatures of exposure appear to fall along one line during the initial stage of exposure of 5 h (Fig. 2). However, the insert in Fig. 2 at magnified

Table 2 Parabolic rate constant of the SASS 904L oxidized at 500–650 °C up to 100 h

Temperature (°C)	ΔW (mg)	Time (h)	k_p ($\text{mg}^2 \text{cm}^{-4} \text{h}^{-1}$)	R^2
500	0.3	0–5	0.03	0.9
	0.6	5–100	0.01	0.97
550	0.7	0–5	0.11	0.94
	0.5	5–100	0.01	0.95
600	1.1	0–10	0.13	0.96
	0.4	10–100	0.01	0.9
650	1.9	0–25	0.17	0.98
	0.2	25–100	0.01	0.96

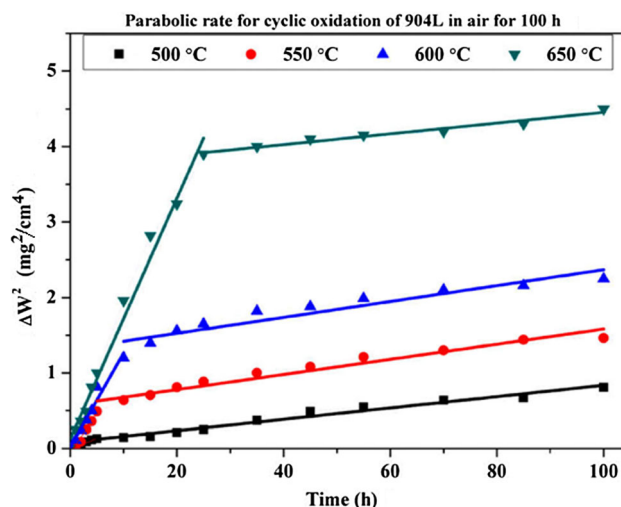


Fig. 3 Variation of square of weight gain per unit area (ΔW)² with time from oxidation of the SASS 904L in air at 500, 550, 600 and 650 °C, up to 100 h

scale reveals increasing slope of ΔW versus t plot with increase in temperature, showing higher rate of weight gain at higher temperatures. The rate of weight gain, however, slowly decreases after the initial period of exposure and become lowest after ≈ 35 h of exposure. Figure 3 shows two distinct segments of high and low slopes in the plots of $(\Delta W)^2$ versus t and indicates fast and slow growth behavior of the oxide layer in the initial and later stage of exposure.

3.3 Phase Analysis

X-ray diffraction patterns of the as-solution-treated sample and those exposed at different temperatures of 500–650 °C are shown in Fig. 4. The XRD pattern of the as-solution-treated sample shows standard peaks of only the austenite (γ) phase (Fig. 4a), whereas of that exposed at 500 °C for 100 h shows also peaks of Cr_2O_3 in addition to peaks of austenite (Fig. 4b) and peaks of $\text{Fe}_2\text{O}_3/\text{Fe}_3\text{O}_4$ along with

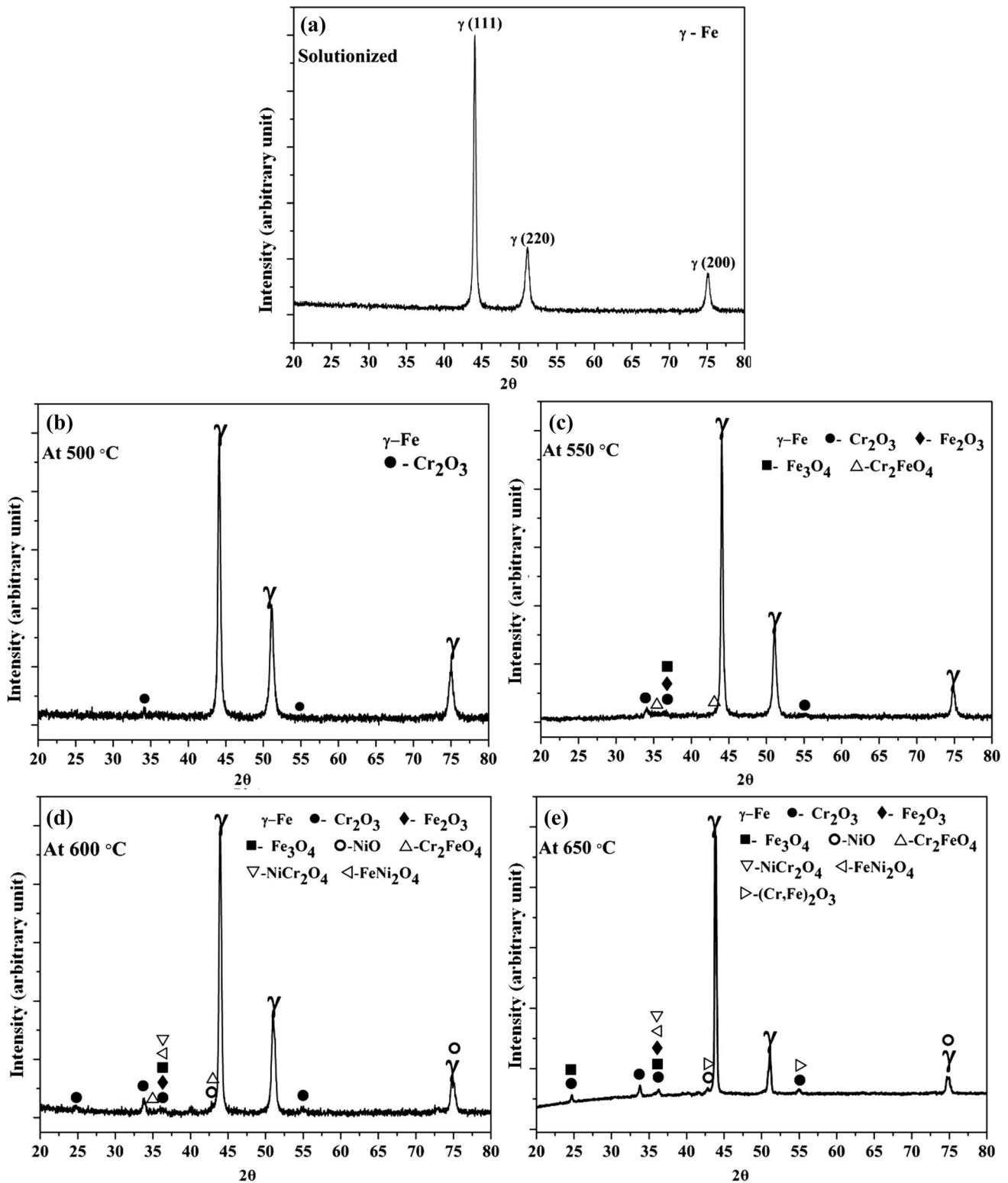


Fig. 4 XRD patterns of the SASS 904L in solution-treated condition (a) and following oxidation with following exposure of 100 h at: **b** 500, **c** 550, **d** 600 and **e** 650 °C

those of austenite (γ) and Cr_2O_3 in the sample exposed at 550 °C (Fig. 4c). The samples exposed at 600 and 650 °C show peaks of austenite (γ), iron oxides (Fe_2O_3 and Fe_3O_4),

chromium oxide (Cr_2O_3), nickel oxide (NiO) and spinels (Fig. 4d, e). The various phases revealed by XRD in the different conditions are listed in Table 3.

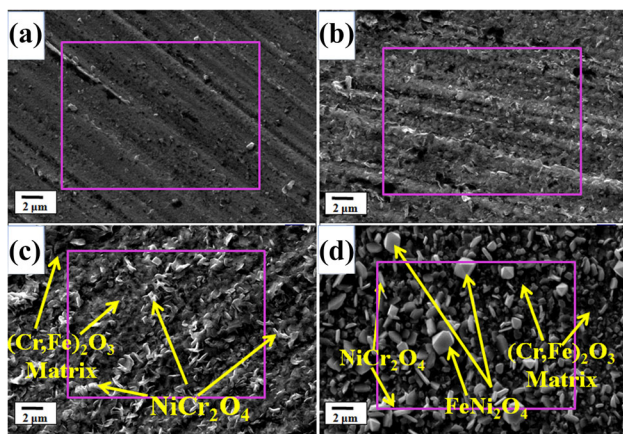
Table 3 Oxide phases formed on the SASS 904L from exposure at 500–650 °C for 100 h in air

Temperature (°C)	Phases
500	γ -Fe, Cr_2O_3
550	Cr_2O_3 , $\text{Fe}_2\text{O}_3/\text{Fe}_3\text{O}_4$
600	Cr_2O_3 , $\text{Fe}_2\text{O}_3/\text{Fe}_3\text{O}_4$, NiO, NiCr_2O_4 , FeNi_2O_4 , $(\text{Cr,Fe})_2\text{O}_3$
650	Cr_2O_3 , Fe_2O_3 , Fe_3O_4 , FeCr_2O_4 , NiCr_2O_4 , FeNi_2O_4 , $(\text{Cr,Fe})_2\text{O}_3$

3.4 Surface Morphology

Surface morphologies of the different samples revealed by SEM–EDS provide important information related to the process of oxidation. Figure 5a–d shows SEM–EDS of the samples oxidized at 500–650 °C, up to 100 h. There is very thin layer of oxide on the surface of the specimen exposed at 500 °C (Fig. 5a), the crests and troughs resulting from the mechanical polishing are quite distinct. The thickness as well as roughness of the surface progressively increases with rise in temperature of exposure from 500 to 650 °C and also there are particles of increasing size (Fig. 5b–d).

There are coarse particles of typical geometrical shapes on the surface of the specimen exposed at 650 °C (Fig. 5d). The various spinels in the matrix are shown in Fig. 5c, d. The composition of matrix at the surfaces, exposed at different temperatures, is tabulated below the SEM micrographs, by EDS analysis of the rectangular enclosed



Temp. (°C)	Compositions are in wt%							
	Mn	Mo	Cr	Ni	Fe	Si	Cu	O
500	0.42	2.22	18.6	21.94	47.26	1.18	1.05	7.31
550	1.69		18.59	20.63	36.87		1.1	21.1
600	1.81	3.65	18.98	14.96	35.01	0.72	2.09	22.77
650	1.88	5.23	22.87	13.49	31	0.97	0.99	23.56

Fig. 5 Surface morphologies of the samples oxidized for 100 h at different temperatures: **a** 500, **b** 550, **c** 600 and **d** 650 °C. Compositional analysis by EDS was carried out from the rectangular enclosed regions

regions. It is relevant to mention that there is no spalling of the surface exposed at 500–650 °C.

Figure 6a–d shows secondary electron image (SE) of the samples exposed at 500, 550, 600 and 650 °C, respectively, with contents of the different elements at marked locations. It may be seen that there is progressive increase in the thickness of the oxidized layer.

3.5 EPMA Mapping of the Cross Section

EPMA analysis of cross sections of the samples exposed from 500 to 650 °C for 100 h is shown in Fig. 7. There is progressive but heterogeneous enrichment of oxygen on surface of the specimens exposed from 500 to 650 °C. Also, there is heterogeneous enrichment of iron on the surface of the samples exposed from 550 to 650 °C. There is enrichment of chromium, covering entire surface of the specimens, exposed at 500–650 °C, without any discontinuity. The thickness of the enriched chromium layer increases with the temperature of exposure, however, uniformity of the outer surface of the enriched layer decreases with increase in the temperature of exposure. There is very less enrichment of nickel, only on surface of the specimen exposed at the highest temperature of 650 °C (Fig. 7d).

4 Discussion

This investigation clearly reveals that in the intermediate-range of temperature, from 500 to 650 °C, there is rapid weight gain in the initial stage of exposure, with increasing rate as well as in amount, with increase in temperature from 500 to 650 °C, in ambient air. The kinetics of oxidation exhibits parabolic rate law with high and low parabolic rate constants, corresponding to the initial and later stage of exposure (Table 2), due to difference in the kinetics of oxidation and the rate of diffusion of metal cations from interior to surface. The process of oxidation starts with interaction of metal cations and oxygen anions at interface of the material and air and leads to the formation of their oxides on surface of the material [3]. Based on the earlier work on chromium containing iron alloys, on the proportion of formed oxides of chromium and iron, it has been observed that the formation of chromium oxides is thermodynamically favored while that of iron oxides is kinetically controlled [11]. Since oxidation temperature and oxygen exposure are known to be the two key factors for the rate of oxidation, surface composition and oxide structures [12, 13], the higher rate and amount of weight gain in the initial stage of exposure, at increasing temperatures may thus be understood. The proportion of the formed oxides at the beginning will also be affected by bulk diffusion coefficients of the different metal cations

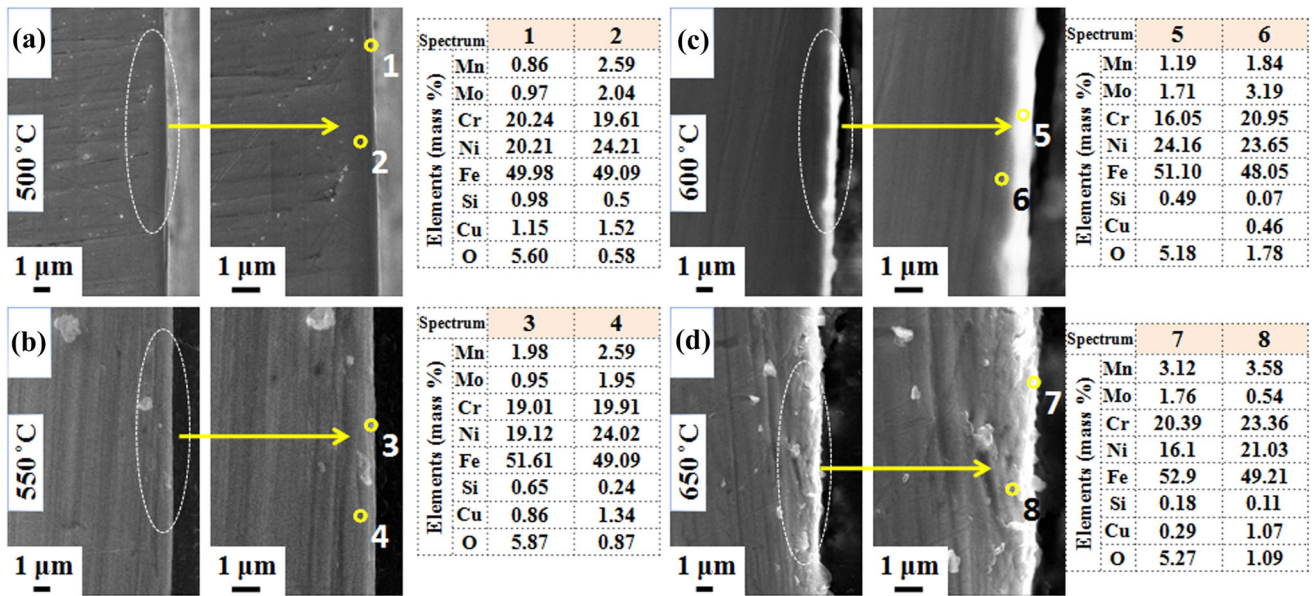


Fig. 6 Cross-sectional SEM–EDS of the samples oxidized at different temperatures: a 500, b 550, c 600 and d 650 °C. for 100 h

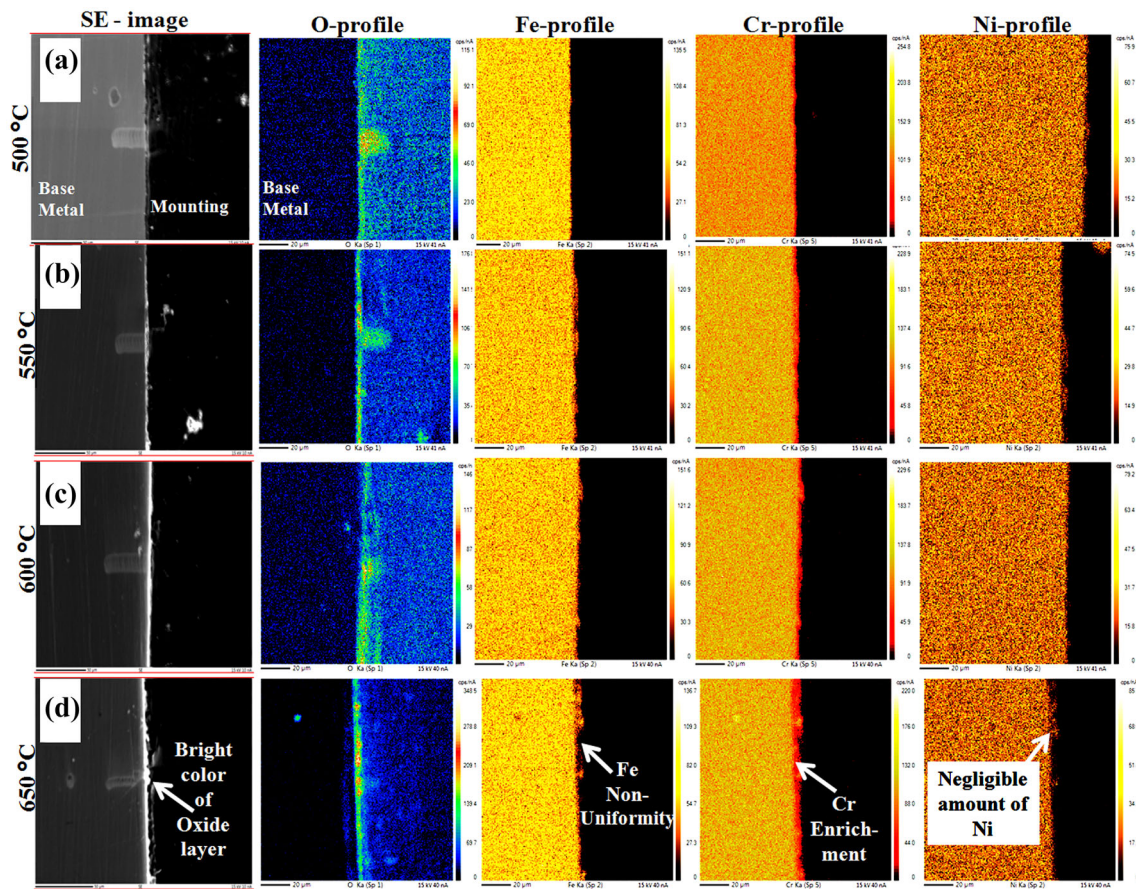


Fig. 7 EPMA analysis of cross sections of the samples exposed at 500–650 °C up to 100 h

Table 4 Standard Gibbs free energy of formation of different oxides

ΔG (in kJ/mole)	Fe_2O_3	Fe_3O_4	Cr_2O_3	FeCr_2O_4	NiO	MnO
ΔG_{500}	– 140.72	– 215.51	– 919.42	– 472.35	– 168.46	– 77.40
ΔG_{550}	– 133.68	– 209.25	– 906.43	– 467.28	– 164.20	– 73.76
ΔG_{600}	– 126.65	– 203.00	– 893.44	– 462.22	– 159.94	– 70.12
ΔG_{650}	– 119.62	– 196.74	– 880.45	– 457.16	– 155.68	– 66.48

through austenitic matrix of the 904L steel. It has been established in the austenite Fe–20Cr–12Ni–Si alloy that at elevated temperature (800–1400 °C), $D_{\text{Cr}} > D_{\text{Fe}} > D_{\text{Ni}}$ [14]. The same trend is found at 500–650 °C, from extrapolation of the high-temperature data of Rothmann et al. [14]. It is presumed that a similar trend would have been also in the austenitic 904L steel. It may be seen from the XRD patterns (Fig. 4) that there is formation of only Cr_2O_3 which appears to be very thin at 500 °C (Figs. 5 and 6), likewise there is very little weight gain (Fig. 2), whereas at 550 °C there is formation of Fe_2O_3 , Cr_2O_3 and spinels of Fe_2O_3 – Cr_2O_3 . At 600 and 650 °C there is formation of additional spinels of different oxides along with Cr_2O_3 and Fe_2O_3 . There is relatively fast growth rate of kinetically controlled iron containing oxides, resulting from rapid oxidation in the early stage. However, subsequent selective oxidation of chromium and formation of Cr_2O_3 because of most negative ΔG value of its formation (Table 4) leads to the formation of a healing Cr_2O_3 layer at the base of the previously formed oxides and spinels, and the further rate of oxidation is drastically reduced due to its strong barrier action. The scales are found intact without any spalling. Further, there is no sign of internal oxidation; therefore, the process of oxidation has been controlled by diffusion of metal cations to outer surface of the scale. Once there is formation of uniform layer of Cr_2O_3 , further process of oxidation is drastically reduced because it is controlled by the rate of diffusion of metal cations through the layer of the protective Cr_2O_3 . It has been established earlier that $D_{\text{Cr}} > D_{\text{Fe}} > D_{\text{Ni}}$ in the Cr_2O_3 layer [15–17]. Since, Cr content in the 904L steel is more than the critical content of 18 wt% [18, 19] for the formation of continuous and protective layer of Cr_2O_3 , this material remains resistant to oxidation from 500 to 650 °C. Due to relatively higher diffusivity of Cr cations and their adequate supply from the substrate, there is a slow but continued growth of Cr_2O_3 , hence the negative effect of lower resistance of spinel of oxides against diffusion of metal cations through them is counteracted. It may further be noted from the distribution of the different elements in the scale (Fig. 7) that the content of other elements as compared to Cr is much less; hence, their deleterious effect as spinels of their oxides, in promoting diffusion of cations through them is

less, even in the later stage of exposure, at least up to 100 h of exposure, observed in the present investigation. The non-uniformity in the thickness of the scale may be attributed to dissimilarity in orientations of the coarse grains of 40 micron mean intercept length. It may be seen in Fig. 3 that there is dual slope of high and low inclination corresponding to initial and later stage of exposure. This behavior is from rapid weight gain in the initial stage due to fast diffusion of Cr, Fe and Ni through the austenite matrix to surface and formation of their oxides. However, in the later stage, the rate of weight gain is reduced due to much slower diffusion of these elements through the protective oxide layer of Cr_2O_3 formed on the surface. This observed behavior of dual slope in the present investigation is in line with the earlier investigation made on Sanicro-25 which is very close in composition to the 904L steel [20–23]. The composition of Sanicro-25 may be seen to be very close to that of 904L, the material of present investigation (Table 1). The faster rate of weight gain in the initial stage may also be assisted by the relatively higher potential of oxygen, from more frequent opening of the furnace in the initial thermal cycles, as compared to later stage cycles of much longer durations.

It may be seen from Fig. 4 that there are strong peaks of γ -phase from all the exposed samples, including the one exposed at the highest temperature at 650 °C. Thus, it is obvious that oxide scales are too thin to stop penetration of X-rays through them to austenite substrate, and all the phases formed from oxidation are exposed to X-rays.

4.1 Oxidation Mechanism

The mechanism of oxidation of the SASS 904L at different temperatures is shown schematically in Fig. 8. At 500 °C, Cr forms a thin layer of Cr_2O_3 due to high affinity of Cr with O_2 (Fig. 8a). With rise in the temperature, at 550 °C (Fig. 8b), Cr_2O_3 layer grows and a layer of iron oxide also forms. This shows a matrix with lean presence of Fe–Cr and Ni–Cr oxide spinel, confirmed by XRD and SEM surface analysis. At 600 °C (Fig. 8c), the dark appearance of the layer shows Fe enrichment over the Cr oxide matrix. In addition to these enrichments, the growth of oxide particles through the matrix occurs, which are rich in Fe, Ni

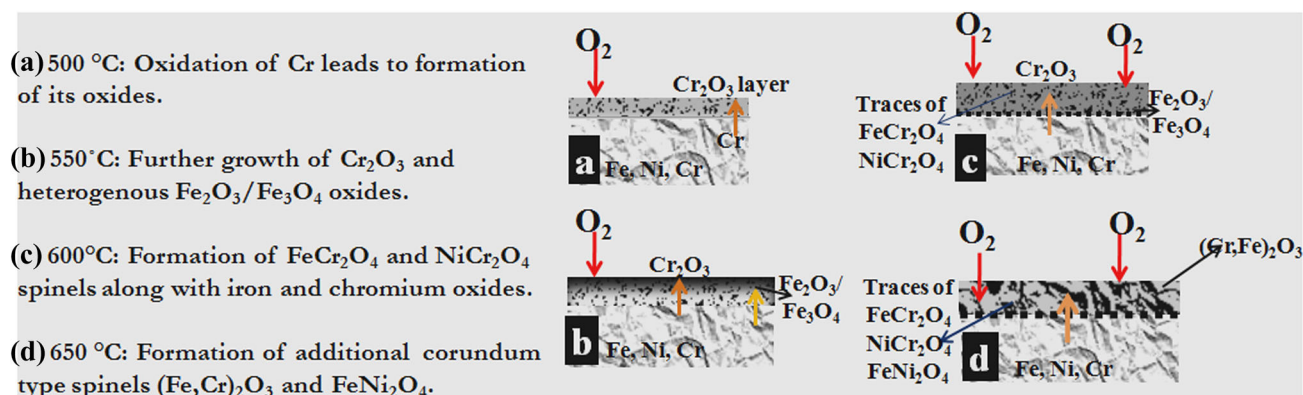


Fig. 8 Schematic process of oxidation of the SASS 904L from 100 h of exposure at different temperatures: **a** 500, **b** 550, **c** 600 and **d** 650 °C

and Cr oxides. At 650 °C, (Fig. 8d), the enriched Fe and Cr combines to form corundum type of oxide $(\text{Fe,Cr})_2\text{O}_3$ and further growth of spinel oxides such as of Ni–Cr and Fe–Ni take place.

5 Conclusions

1. Cyclic oxidation of the SASS 904L from 500 to 650 °C for 100 h exhibited parabolic rate law of oxidation in still air. Oxidation rate was fast in the initial stage, increased rapidly with rise in temperature but reduced drastically in the later stage of oxidation.
2. There was no sign of spalling of the scale and internal oxidation below the substrate. The oxidation resistance under cyclic oxidation was found to be good up to the investigated exposure of 100 h.
3. There was formation of Cr_2O_3 at 500 °C; Cr_2O_3 , Fe_2O_3 , spinel of $\text{Fe}_2\text{O}_3\text{--Cr}_2\text{O}_3$ at 550 °C; and several other spinels of different oxides at 600 and 650 °C.

Acknowledgements The authors are thankful to Prof. N V C Rao and Dr. Dinesh Pandit, Department of Geology, Institute of Science, B.H.U., Varanasi for providing EPMA facility.

References

1. Lepingle V, Louis G, Allué D, Lefebvre B, and Vandenberghe B, *Corros Sci* **50** (2008) 1011.
2. Momeni A, and Dehghani K, *Metall Mater Trans A* **42** (2011) 1925.
3. Wallwork G R, *Rep Progress Phys* **39** (1976) 401.
4. Lai J K L, Shek C H, and Lo K H, *Stainless Steels: An Introduction and Their Recent Developments*, Bentham Science Publishers, Sharjah (2012).
5. Calmunger M, *On High-Temperature Behaviours of Heat Resistant Austenitic Alloys*, Linköping University Electronic Press, Linköping, (2015).
6. Schade C T, Schaberl J W, and Lawley A, *Int J Powder Metall* **44** (2008) 57.
7. Sedriks A J, *Int Met Rev* **27** (1982) 321.
8. Dillon C P, *Corrosion Resistance of Stainless Steels*, CRC Press, Boca Raton (1995).
9. Sequeira C A C, Brito P S D, Antunes R M M, Neto R P C, and Rodrigues L F F T T G, in *Conference on Materials in Oceanic Environment, Euromat' 98*, At Lisbon (1998), vol 1, p 631.
10. Cao Y, and Norell M, *Oxid Met* **80** (2013) 479.
11. Allen G C, Harris S J, Jutson J A, and Dyke J M, *Appl Surface Sci* **37** (1989) 111.
12. Lampimäki M, Lahtonen K, Jussila P, Hirsimäki M, and Valden M, *J Electron Spectrosc Relat Phenom* **154** (2007) 69.
13. Ali-Löyty H, Jussila P, Hirsimäki M, and Valden M, *Appl Surface Sci* **257** (2011) 7783.
14. Rothman S J, Nowicki L J, and Murch G E, *J Phys F Met Phys* **10** (1980) 383.
15. Tan L, Yang Y, Allen T R, and Busby J T, in *Proceedings of the 15th International Conference on Environmental Degradation of Materials in Nuclear Power Systems—Water Reactors*, Springer, pp 1909–1922 (2011).
16. Million B, Růžičková J, and Vřešťál J, *Mater Sci Eng* **72** (1985) 85.
17. Lobnig R E, Schmidt H P, Hennesen K, and Grabke H J, *Oxid Met* **37** (1992) 81.
18. Basu S N, and Yurek G J, *Oxid Met* **36** (1991) 281.
19. Birks N, Meier G H, and Pettit F S, *Introduction to the High Temperature Oxidation of Metals*, Cambridge University Press, Cambridge, (2006).
20. Intiso L, Johansson L-G, Canovic S, Bellini S, Svensson J-E, and Halvarsson M, *Oxid Met* **77** (2012) 209.
21. Zurek J, Yang S-M, Lin D-Y, Hüttel T, Singheiser L, and Quadkners W J, *Mater Corros* **66** (2015) 315.
22. Rutkowski B, Gil A, Ratuszek W, Woźnik B, and Czyrska-Filemonowicz A, *Inżynieria Materiałowa* **37** (2016) 223.
23. Koech P K, and Wang C J, *Oxid Met* **90** (2018) 713.

Publisher's Note Springer Nature remains neutral with regard to jurisdictional claims in published maps and institutional affiliations.